Chapter 3

Experimental Apparatus

3.1 The Large Hadron Collider (LHC)

To search for the Higgs particle and some new physics at 14 TeV, the Large Hadron Collider will collide current of bunches of protons with a design luminosity $\mathcal{L} = 10^{34}\ \mathrm{cm}^{-2}\mathrm{s}^{-1}$. Within the next three years after an initial running, the LHC will be able to provide a full coverage of collision up to the TeV energy scale. Whether or not the Higgs boson exists or whatever the source of the electroweak symmetry breaking, some detectable evidences must be unveiled under the collision energies below 1 TeV [22].

The construction of the LHC beam line will use the old 27-km-long tunnel system of the Large Electron-Positron (LEP) Collider which is located across the Swiss-French border in the north of Geneva, Switzerland. In Table 3.1, we give some important characteristics of the LHC. In Fig. 3.1, the outline of the LHC machine and its sub-accelerators are illustrated. More detail information of the LHC can be found in Ref. [23].

In this section, we give some brief overview of the main components of the machine, in order from injection process to the end of the fill process.

1. **Injection** The old injection system and infrastructure of LEP will be used to empower the LHC. The LHC energy build-up chain starts at a small linear accelerator, which provides the proton beam of primary energy of 50 MeV and boost it up to 1.4 GeV. Next, the Proton Synchrotron (PS) increases the beam energy to 25 GeV and injects it to the Super Proton Synchrotron

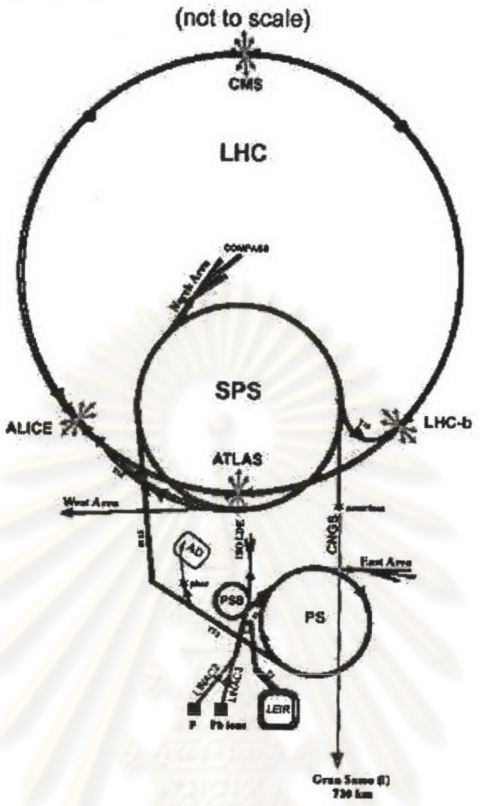

Figure 3.1: The sub-accelerators and the injection system of the LHC. (picture from the LHC Conceptual Design, CERN/AC/95-05, 1995.)

(SPS). After being accelerated to 450 GeV, the beam is then transferred to the LHC

2. **Vacuum system** The proton beam runs inside a circular tube made of stainless steel under the LHC vacuum system. The vacuum state is achieved by the running flow of 1.9 K super-fluid helium around the tube. For problem involving heat load from the beam radiation which is caused by the synchrotron light, there is a special beam screen protection to absorb it.

3. **Magnet** The quality of magnet system of a collider indicates how high energy the collider can attain. For the LHC, the LHC superconducting dipole magnets are expected to attain the field as high as 8.4 T which will induce the beam energy of 7 TeV according to Eq. (3.1):

Table 3.1: The main LHC characteristics

Beam and interaction characteristics		
Beam Energy	(TeV)	7
Luminosity	($cm^{-2}s^{-1}$)	10^{34}
Time between collisions	(ns)	25
Bunch length	(cm)	7.7
Beam radius at interaction point	(μm)	15.9
Technical characteristics		
Ring Circumference	(m)	26658.9
RF frequency	(MHz)	400.8
Number of bunches	-	2835
Number of bending dipoles	-	1232
Magnetic length of the bending dipoles	(m)	14.2
Field of the bending dipoles	(T)	8.386
Bending radius	(m)	2784.3
Temperature of the main magnets	(K)	1.9

$$P_T = 0.3BR = 0.3 \cdot 8.386 \cdot 2784.3\,GeV = 7.0\,TeV \tag{3.1}$$

where R (m) is the bending radius of the proton beam and P_T is the transverse momentum (see Appendix A.3).

Even though only one kind of magnets would be enough to carry the beam of antiprotons and protons, it is not feasible to produce enough amount of antiprotons to attain the high luminosities which are needed to fully exploit the physics potential at 14 TeV. Thus, the LHC has installed a twin bore magnet in which two beams of protons can circulate under the same mechanical design and cryogenics system.

4. **Cryogenics** The LHC cryogenics system uses niobium-titanium as superconducting cable which is maintained under the temperature of 1.9 K by a flow of super-fluid helium. The super-fluid helium has an advantage over normal liquid helium (4.2 K) for its higher heat conductivity and lower viscosity. At 1.9 K temperature, a high magnetic field of 8.4 T can be achieved.

5. **RF system** The radio frequency (RF) system of the LHC will be located at one of the eight insertions of the LHC ring. Each beam will use separate set of RF system, providing frequency of 400.8 MHz. This high frequency will correspond to the time interval of 2.5 ns between the RF bucket. Bunches of protons filled by every tenth of this bucket will be separated by 25 ns.

6. **Interaction points** The two locations of two general purpose detectors A Toroidal LHC ApparatuS (ATLAS) [24] and CMS [25] will host the two highest luminosity interaction points of the proton bunch currents. The other two detectors, the heavy-ion experiment A Large Ion Collider Experiment (ALICE) [26] and the B-Physics experiment the Large Hadron Collider beauty experiment (LHCb) [27], will host other lower luminosity interaction points.

7. **Beam cleaning** In a high luminosity beam, there will be a halo of particles elastically scattered away from the beam area. These particles will deposit their energies to the surrounding material which could damage the magnet system. At the LHC, a collimators system is installed to absorb these particles to keep material parallel to the beam line from being damaged. Two beam cleaning systems are installed at the LHC.

8. **Beam dump** In beam dumping process, a kicker magnet will first extract the beam from the main ring. The beam is then defocused and transported to a dump block of graphite surrounded by heavier materials at the end of the 750 m transfer tunnel. During transportation, the beam's cascade will be diluted and the radiation from the beam will be shielded.

3.1.1 The LHC experimental environment

The major characteristics of the experimental environment of the LHC lie in its high luminosity and a short bunch crossing interval.

High luminosity is the same meaning as high collision rate. In a proton-proton collision, the interactions occur among the proton's constituents – the valence quarks, gluons and the sea quarks. The amount of energy created from the collision of the protons is determined by the fraction of the total proton energy carried by its constituents. There is a large difference in order of magnitude between the cross-sections for inelastic interactions and the cross-section of the interesting events (for example the Higgs production).

For example, at the luminosity of $\mathcal{L} = 10^{34}$ cm^{-2}s^{-1} and a fraction of 2835 out of 3564 bunches filled by the LHC, an inelastic interaction which has the cross-section $\sigma = 55$ mb [28] will have, on the average of one bunch crossing, the number of collision

$$n = \mathcal{L}\sigma\frac{3564}{2835}\tau = 10^{34}\,cm^{-2}s^{-1}\cdot 55\,mb\cdot\frac{3564}{2835}\cdot 25\,ns = 17.3, \qquad (3.2)$$

where τ is the bunch-crossing interval of the protons.

Due to the result from large particle multiplicity per event, there will be many *minimum bias* events piled up on top of every interesting event. The minimum bias events are the majority of interactions from fusion processes of gluons or quarks with a small energy transfer. They are detected as hadrons of low momentum and nothing else. At the scale of LHC energy, this minimum bias events will lead to a huge amount of particle density in the detector.

Because of high interaction rate and short bunch interval, the trigger and data acquisition system of the detectors must be of high level of computing capability. They have to meet the requirement of identifying interesting events and store them in a time correspond to the bunch crossing an interval of 25 ns. At this high rate, storing all the events is not feasible; therefore the multi-level trigger system is implemented to reduce the data volume from the collision rate of 40 MHz to the level 1 maximum trigger rate of 100 kHz. The types of particles observed by the trigger system are isolated leptons, photons or electrons in the electromagnetic calorimeter and muons in the muon system, jets or missing transverse energy in the combined calorimeter system. The first level determination to select an event will be under the requirement of these trigger objects.

Another main feature of the design of the LHC is the radiation protection system. In a high rate of proton-proton collisions, intense radiation always presents. While most of the products from collision are absorbed in the calorimeters, backscattered particles and shower tails will still cause danger everywhere in the detector. Especially in the inner detector and the forward region of the experiment, the dose rates and particle fluence are at their highest intensity. Radiation resistance is therefore of the crucial criteria for all detector components at the LHC.

3.2 The Compact Muon Solenoid (CMS)

The CMS detector is one of the general purpose detectors built for supporting particle physics experimental program at the LHC. This thesis has made an investigation based on the CMS geometry, material, electronics, etc, to study the possibility of using the $W^{\pm}$ and Z^0 production for luminosity measurement. Therefore, in this section, we give some brief overview of the detector and some physical and technical explanations of its major components. Most technical terms, pictures and the descriptions are excerpted from the CMS Posters [29].

3.2.1 An Overview of the CMS Detector

The CMS detector is designed to run at the highest luminosity at the LHC with a primary goal to hunt for the Standard Model Higgs boson. The CMS is an abbreviation of the Compact Muon Solenoid [25]. The name "Compact" comes from its unique design to confine most of the crucial parts of the detector inside the sophisticated superconducting "Solenoid" magnet. The name "Muon" comes from the muon system of the detector which is of the most important part for detecting and measuring Higgs and other interesting signal that yield muons as their final product. At its completion, the detector will weigh about 12500 ton and cost around 452 million Swiss Francs (MCHF) at 1995 prices. In order to connect with the LHC beam line, the CMS detector will be put about 100 m underground in the caverns.

With the goal of looking for the Higgs boson particle, the CMS detector is optimized to reach a full detecting capability over a mass range of 90 GeV/c^2 to 1 TeV/c^2. In addition, the detector is optimized for capturing various kind of unexpected physics phenomena beyond the Standard Model such as Supersymmetry or Extra Dimension. Furthermore, CMS will be capable of providing insight on the study of beauty and top quarks at lower luminosities and will accommodate many important aspects of the heavy ion physics experiment.

The dimension of the CMS detector is 21.6 m in length and 14.6 m in diameter. Considering the size of particles of about *attometer* ($\approx 10^{-18}$ m), the dimension of the CMS is about 20 order larger in magnitude. This proportion is about the ratio of the size of a giant panda and the size of the milky way.

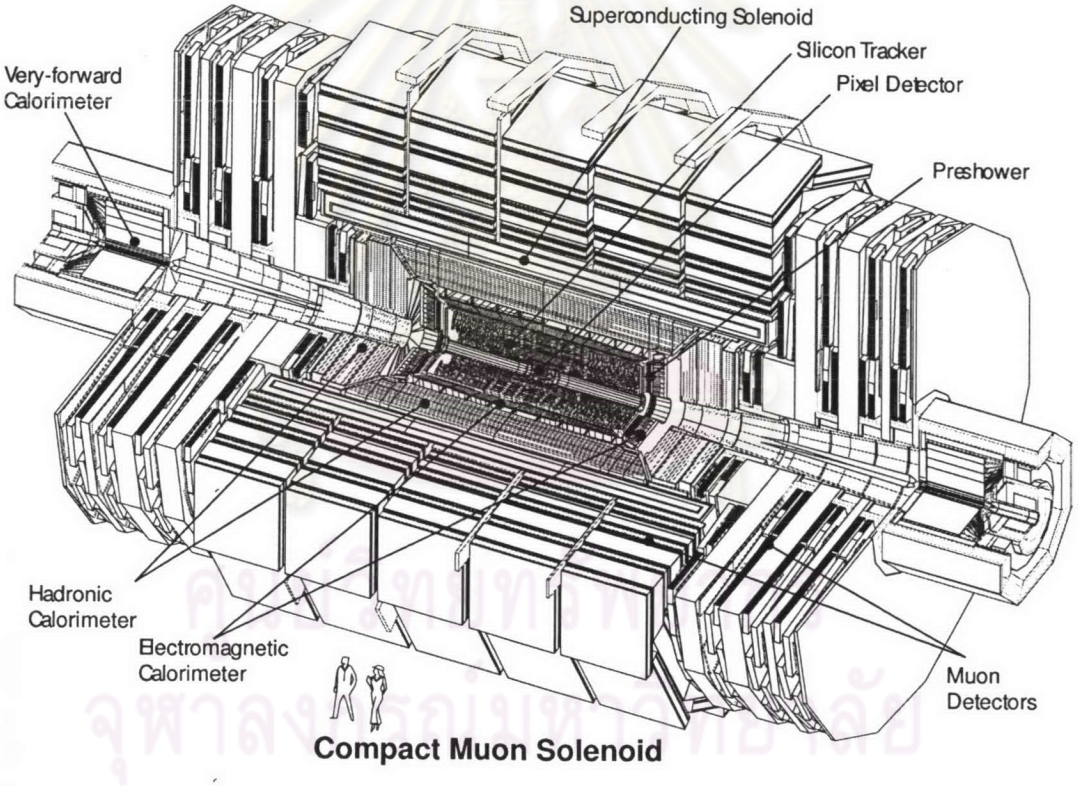

Figure 3.2: The CMS Detector with its components labelled. (picture from http://cmsdoc.cern.ch)

At the CMS, the energy resolution for measuring particles generated by the LHC will be better than 1% at 100 GeV. A CMS's large superconducting solenoid

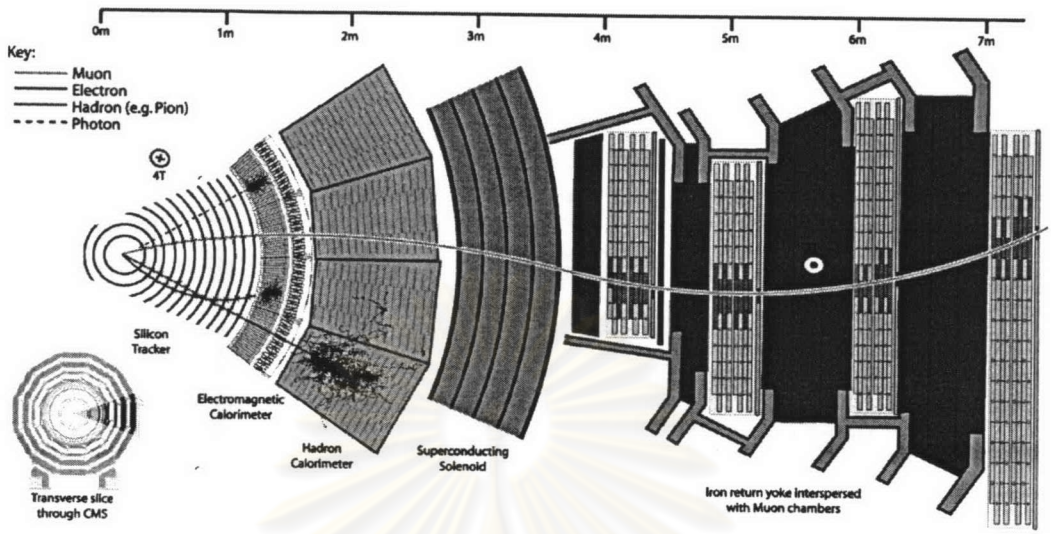

Figure 3.3: Slice of the CMS detector. (picture from http://cmsdoc.cern.ch)

of radius $r \sim 2.9$ m is expected to generate a uniform magnetic field of 4 Tesla. This size of solenoid coil enables a compact design for the muon system up to pseudorapidities of 2.5 without reducing the momentum resolution.
The four major components of the detector, from inside out are: the Tracker, the Electromagnetic Calorimeter (ECAL), the Hadron Calorimeters (HCAL) and the Muon Chamber. Except for the muon chamber, all other components are confined within the solenoid coil, as shown in Fig. 3.2 and Fig. 3.3. In Fig. 3.2, one quarter of the detector taken out to show each important component inside the CMS detector. Fig. 3.3 shows the pie of cross-sectional slice of the CMS and the tracks of different kinds of particles – muon, electron, hadron, photon – those will be caught by each layer of the detector.

The four major components of the detector will be described in detail in the subsections below.

3.2.2 The Tracker

The Tracker of the CMS provides precise momentum measurement for energetic leptons in search for decay signal involving Gauge bosons, $W^{\pm}$ and Z^0. The measurements made by the tracker are combined with track segment reconstructed

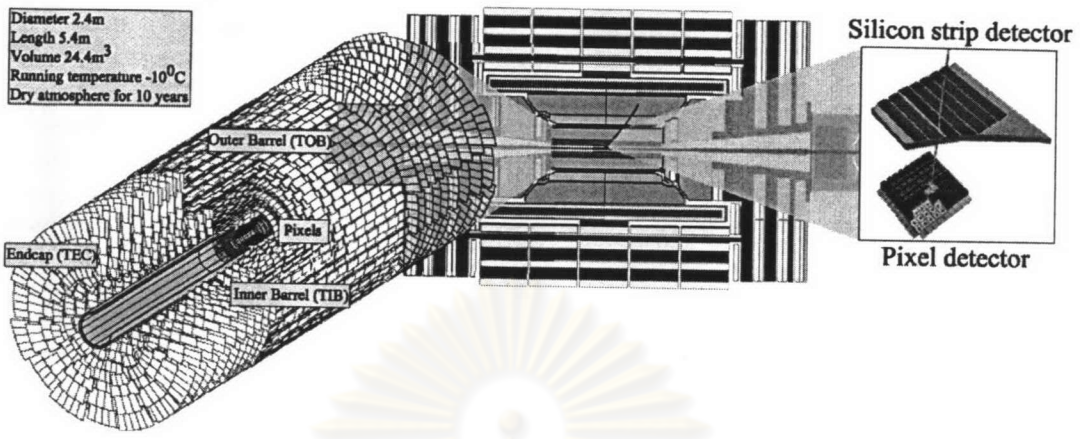

Figure 3.4: The CMS Tracker.

in the outer muon system to cover more of the kinematic region and to increase the precision of muon momentum. The Tracker is not only able to identify and reconstruct isolated leptons and photons, but also able to establish that they are really isolated ones.

The shape of the Tracker is a cylinder, as shown in Fig. 3.4, of 6 m in length and 1.2 m in radius. Inside the volume, a uniform magnetic field of 4 Tesla along the beam axis (z-axis) is presented. The tracker covers rapidity in range of $\mid \eta \mid < 2.5$. The definition of η as well as an illustration showing a scale of η of the CMS detector is displayed in Fig. A.3 in Appendix A.

All high transverse momentum P_T charged particles produced in the central rapidity region are reconstructed with a momentum precision of $\delta P_T/P_T \approx 0.005 \bigoplus 0.15 P_T$ (P_T in TeV). Combining the tracking system with the outer muon chamber system, the resolution of the measurement of the momentum of muons above 100 GeV is enhanced to more than 10%.

Most of the tracker material is made of silicon. Silicon is widely used to make a semiconductor detector material because it could provide the highest energy and spatial resolution, and give excellent response time. The basic operation of the tracker is the following: when a charged particle penetrates the semiconductor detector, it causes electron-hole pairs along its track. The more the loss of the energy, the more electron-hole pairs being created. Electric field is applied to separate the electron-hole pairs before they recombine; the electrons then drift

towards the anode while the holes move toward the cathode. The charges are collected by the electrodes and they produce a current pulse on the electrode corresponding to the measurement of the deposited energy.

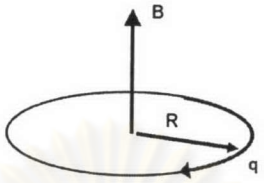

Figure 3.5: The diagram showing the magnetic field (B) being perpendicular to the plane of particle's circular motion of radius R.

In the Tracker, the measurement of momentum of charged particles utilizes the concept of bending of the track trajectory in the magnetic field. Inside the Tracker, for a charged particle with velocity v perpendicular to a magnetic field of strength B (in Tesla) circulating in a circle of radius R (in meters), as shown in Fig. 3.5. The transverse momentum (P_T) perpendicular to the B field measured in GeV/c, is calculated by a formula $P_T = 0.3\ B\ R$.

The CMS Tracker composes of three sub-detector elements, arranged in concentric cylindrical volumes: the Pixel Detectors, Silicon Strip Detectors (SST) and Micro Strip Gas Chamber (MSGC), from innermost to the outermost respectively.

Pixel Detectors

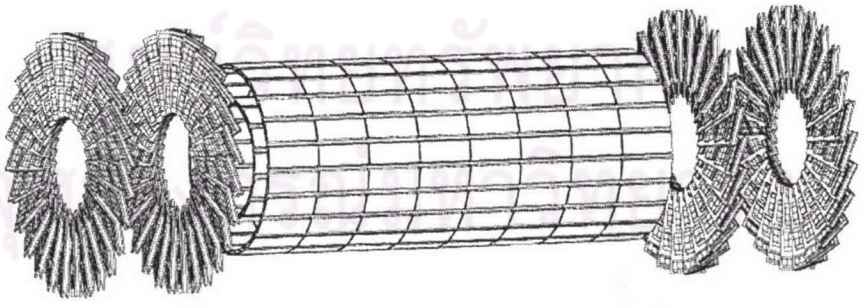

Figure 3.6: The Pixel Detector Layout.

A Pixel Detector, as shown in Fig. 3.6 is a semiconductor type made of wafers with small rectangular two-dimensional elements of linear size less than a

millimeter. The detector consists of large number of those elements to ensure high spatial resolution in two coordinates.

The two barrel layers of Pixel Detectors of the CMS are located at the smallest radius from the beam line. Its two endcap disks cover radii from 6 cm to 15 cm. Each layer of the pixel consists of modular detector units which are made of thin, segmented sensor plates. Each unit is implemented with highly integrated readout chips connected to them using a bump bonding technique.

Silicon Strip Detectors

The Silicon Strip Detector is constructed in layers as show in Fig. 3.7. The layers are separated into the inner barrel layers (TIB) and the outer barrel layers (TOB). The inner barrel (TIB) layers compose of four layers: a double sided layers 1 and 2 and two inner endcaps (TID), each composed of three small disks. The outer barrel (TOB) structure composes of six concentric layers, arranging from nearest to the tracker towards the calorimeter.

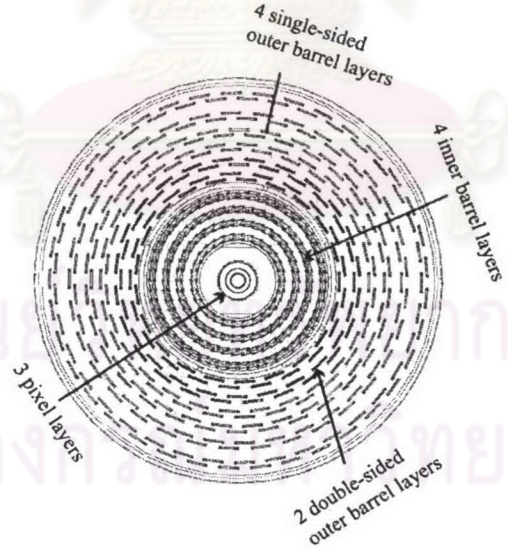

Figure 3.7: The Silicon Strip Detector Layout.

Two endcaps (TEC) (as shown in Fig. 3.4) of the Silicon Strip Detectors cover a rapidity range $|\eta| < 2.5$. The endcap modules are mounted in 7 rings on

2×9 disks consisting of wedge shaped petals. The 1, 2 and 5 detector rings are double sided, with each side acting as sensors. One of the sides is placed in an angle of 100 mrad with respect to the other side so that the module can provide information of the azimuthal angle (ϕ) coordinate.

Silicon sensors possess a capability of fast response and small pitches, covering the range from 80 to 205 μm. This feature makes silicon suitable for high occupancy and high resolution experiments.

Micro Strip Gas Chamber

The MSGCs of the Tracker provide an intrinsic spatial resolution better than 40 μm and a hit efficiency better than 98%. It has a cylinder shape with dimension of 6 m in length and 3 m in diameter and provides an average number of 6 hits per track with readout pitch of $\sim$ 200 μm and a strip length between 10 and 25 cm. The MSGC is a gas proportional counter associated with micro-electronics technology and millions of individual detection elements (strips). In the MSGC, the distance between the sensing electrodes (the anode strips) is typically 200 μm providing an accuracy much better than 1 μm. The spreading of the charge on more than one strip, due to the effect of diffusion, allows the use of interpolating algorithms to achieve a position resolution much better than the one dictated by the readout pitch. This is the main advantage of gas micro-strip detectors with respect to solid-state micro-strip detectors. It is allowed to cover large areas with a reasonable number of electronic channels. However, the main disadvantage of the MSGC is the speed of primary charge collection that cannot be easily reduced below two LHC bunch-crossings.

3.2.3 The Electromagnetic Calorimeter

The CMS electromagnetic calorimeter (ECAL) is the most important part to study the electroweak symmetry breaking, especially the Higgs aspect. The ECAL of the CMS is designed to provide a measurement of two-photon decay mode for $m_H \leq 150$ GeV, and a measurement of the electrons and positrons from the decay of Ws and Zs originating from the $H \rightarrow WW$ and $H \rightarrow ZZ$ decay chain under

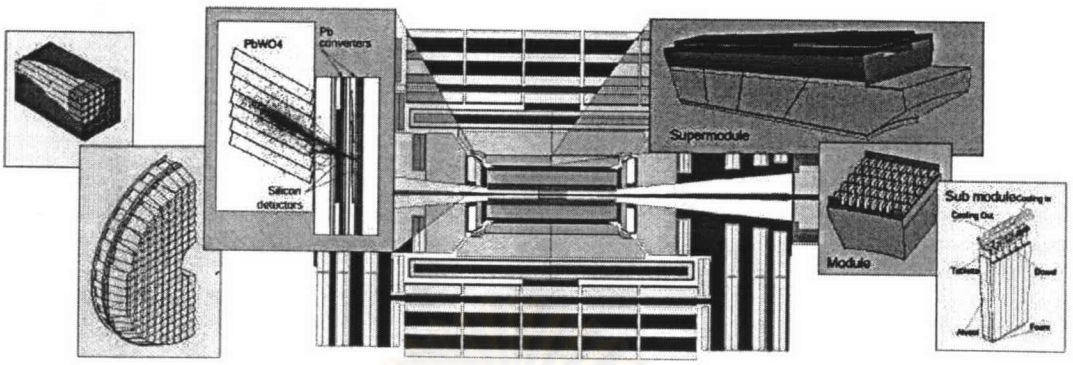

Figure 3.8: The CMS's Electromagnetic Calorimeter.

140 GeV $\leq m_H \leq$ 700GeV. The homogeneous characteristic of the calorimeter also allows good measurement of events with missing transverse energy, due to undetected neutrino-like particles.

The typical electromagnetic interactions of high-energy that occur in the ECAL are:

- Bremmsstrahlung (photon emission in deacceleration or acceleration),
- Bhabha scattering (electron-positron scattering),
- Coulomb scattering (e.g. electron-nucleon scattering),
- Annihilation (e.g. $e^+e^- \rightarrow \gamma\gamma$),
- Pair production ($\gamma \rightarrow e^+e^-$),
- Decay of π^0,
- Compton scattering (photon-electron scattering),
- Möller scattering (electron-electron scattering).

Bremsstrahlung and electron pair production are the most dominant processes for high-energy electrons and photons; their cross-sections become nearly independent of energy above 1 GeV. These dominant electromagnetic processes combining with the small fluctuation help distinguish electromagnetic showers from hadronic showers decisively.

The secondary particles produced in the electromagnetic processes are mainly e^+, e^- and γ; most of the energy is consumed for particle pair production. The cascade develops through repeated similar interactions. The shower maximum, with the largest number of particles, is reached when the average energy per particle becomes low enough to stop further multiplication. From this point, the shower decays slowly through ionization losses for e^-, or by Compton scattering for photons. Nuclear interactions such as photonuclear effects are negligible at this step.

There are two main components for the ECAL of the CMS. One is the main feature of ECAL which is made of Lead-Tungstate crystals, a scintillating material; another is a Preshower Detector located at the endcap, as shown in Fig. 3.8. Both components will be described in more detail in the following subsections.

Lead-Tungstate Crystals

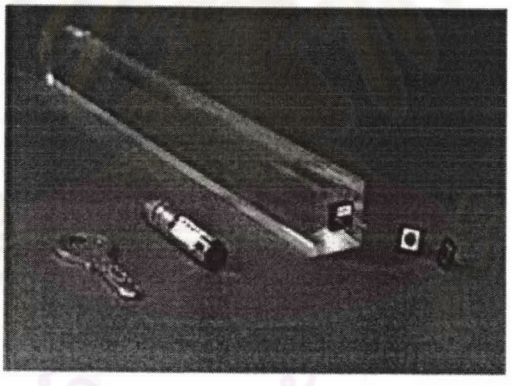

Figure 3.9: The lead-tungstate crystals have a front face of about 22×22 mm^2 and have a length of only 23 cm

More than 80,000 of lead-tungstate ($PbWO_4$) crystals installed with avalanche photodiodes or vacuum phototriodes and associated electronics are installed in the ECAL system, as shown in Fig. 3.9.

The basic operation of the scintillating crystal is the following: when charged particles go through the scintillating material, they excite the molecules of the material. When electrons of the excited molecules fall back to its ground state,

they emit short light pulse which will be amplified, converted and interpreted by electronic system.

Lead tungstate crystals are material of choice for the CMS because they offer short radiation length and a small Molière radius, allowing a very compact electromagnetic calorimeter construction. Also, the material can be produced from readily available raw materials and substantial experience of production.

To convert energy of charged particles to electronic signal, the scintillation light from $PbWO_4$ is first detected by silicon avalanche photodiodes (APDs) in the barrel region (EB, $\mid \eta \mid < 1.48$) and vacuum phototriodes (VPTs) in the endcap region (EE, $1.48 < \mid \eta \mid < 3.0$). In this process, energy is converted to light. Then, the light is converted into a photocurrent by the photodetector. The relatively low light yields a small current which is amplified by preamplifier and converted into a voltage waveform. The signal is then acquired and digitized. Finally, the electronic data are transported off the detector via optical fiber to the upper-level readout. The diagram of the electronic readout sequence is shown in Fig. 3.10.

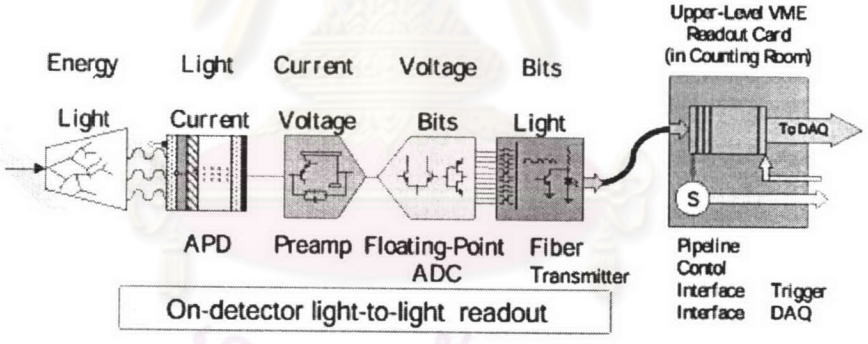

Figure 3.10: A diagram showing the electronic readout sequence in ECAL.

Preshower Detector

A Preshower detector consists of two components: a barrel detector and an endcap detector, as show in Fig. 3.11. The barrel detector covers the rapidity range from $\eta = 0$ to $\eta = 0.9$. Its major function is to provide a measurement of the photon angle in the η direction. The endcap detector covers the rapidity range from about $\eta = 1.65$ to $\eta = 2.6$ and its major operation is to provide $\gamma - \pi_0$ separation.

Both barrel and endcap contain thin lead converters followed by silicon strip detector planes, positioned in front of the ECAL. The measurement of the energy deposition in the 2 mm pitch silicon strips allows the determination of the impact position of the electromagnetic shower. In order to maintain the excellent energy resolution of the ECAL, the energy measurement in the silicon is used to apply a correction to the energy measured in the crystals, thus correcting for the energy deposited in the lead converters.

The two preshower detectors have many similar structure, particularly the front-end electronics and readout. The endcap preshower detector and the barrel preshower will be described in more detail below.

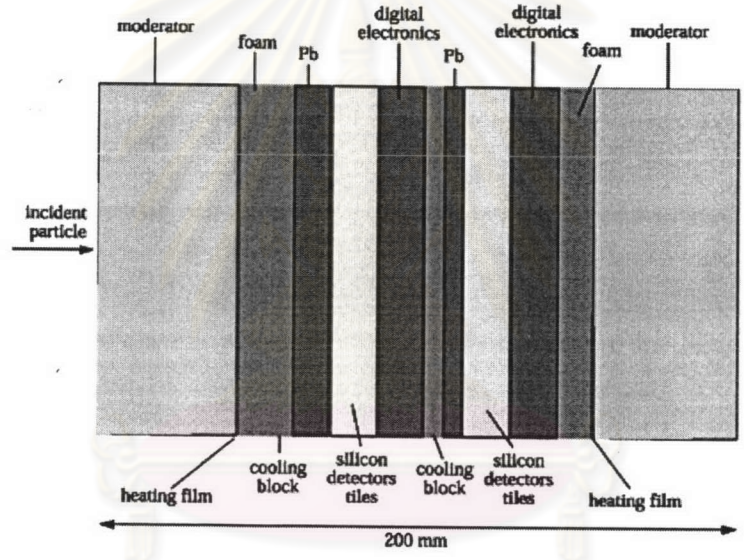

Figure 3.11: The preshower detector contains two thin lead converters followed by silicon strip detector planes placed in front of the ECAL.

Endcap Preshower The primary function of the endcap preshower is to provide $\gamma - \pi_0$ separation in the forward region: in about half of the $H \rightarrow \gamma\gamma$ decays, one of the photons will fall in the rapidity interval covered by the endcaps. At this rapidity, the high energy of the π_0 results in two closely-spaced decay photons indistinguishable from a single-photon shower in the crystal ECAL.

The endcap preshower covers the rapidity interval $1.653 < \eta < 2.6$. Its inner and outer radii are 457 mm and 1230 mm respectively. The endcap preshower is

a planar structure.

Barrel Preshower The main goal of the barrel preshower detector is to measure the photon angles in the η direction at high luminosity, which is needed for the search of the Higgs decaying to two photons. The detector modules are similar to those used in the endcap preshower, with the difference that, each module contains two adjacent silicon detectors connected by bonding to form long strips.

3.2.4 The Hadronic Calorimeter

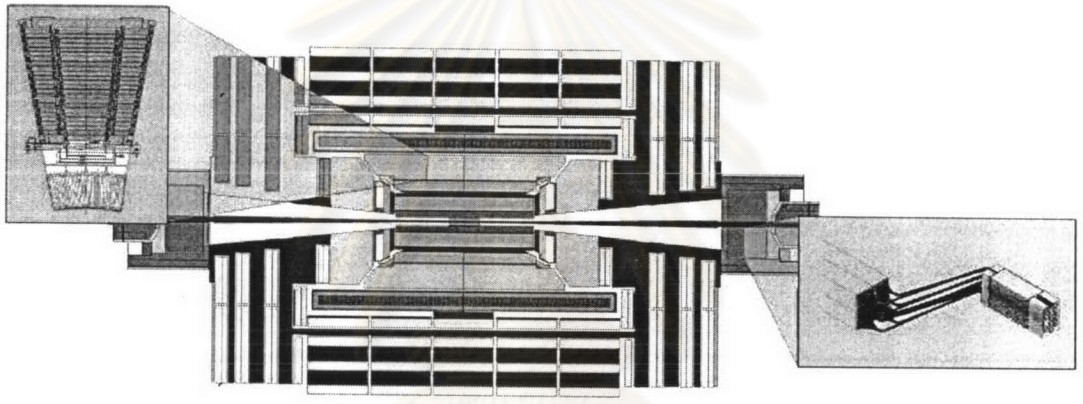

Figure 3.12: The CMS's Hadronic Calorimeter.

The CMS hadronic calorimeter (HCAL), as shown in Fig. 3.12, measures directions and energy of quark, gluon and neutrino. For neutrino, its energy and directions are measured by the jets and of the missing transverse energy. The determination of missing energy provides important signature for new particles and phenomena, such as those in the searches for the supersymmetric partners of quarks and gluons. Particles such as electrons, muons, or photons are identified by the hadronic calorimeter in combination with the electromagnetic calorimeter and the muon system.

In high energy collision, the hadronic interaction is mostly dominated by a succession of inelastic hadronic interactions. These are characterized by multiparticles production and particles emission originating from nuclear decay of excited nuclei. Furthermore, there are frequent generations of π^0's which leave an

electromagnetic component present in hadronic showers. The secondary particles produced in hadronic interactions are mostly pions and nucleons. Other important secondary particles are groups of particles called *jets*. The jets are produced in highly collimated form as a consequence of hadronization of partons (quarks and gluons) produced in hard collisions. They vary widely in shapes, particle contents and energy spectrums.

The HCAL of CMS is made of non-magnetic material, copper alloy and stainless steel. The intrinsic high density of copper makes it suitable for being an absorber material.

Shown in the Fig. 3.13, the components of the HCAL consist of three parts: Barrel (HB), Endcap (HE) and, at the endcap region of the CMS detector, the Forward Calorimeter (HF).

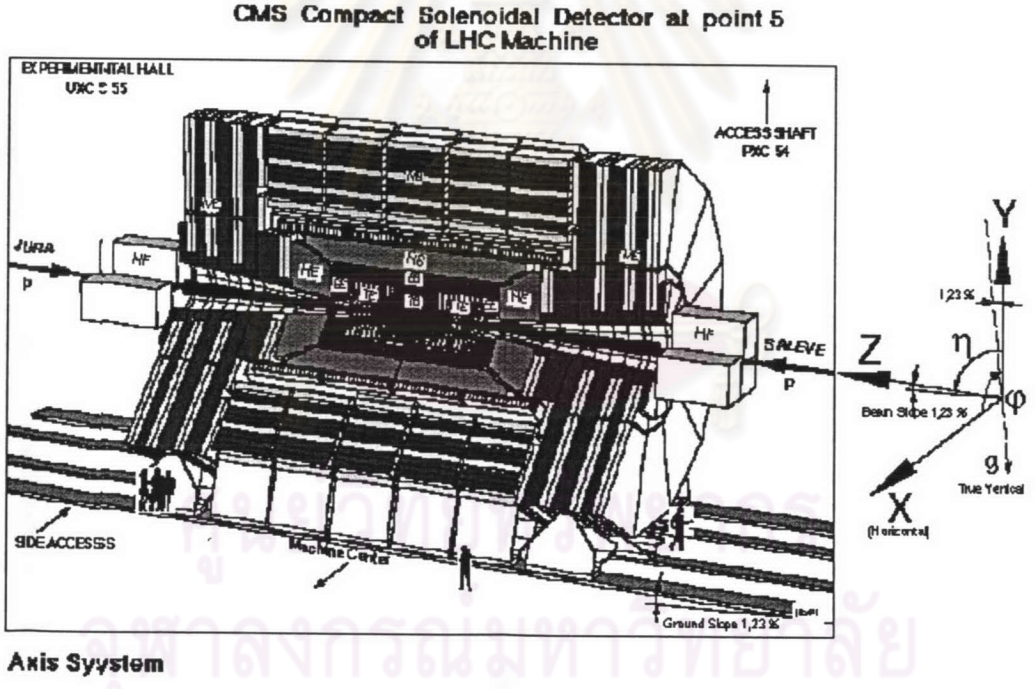

Figure 3.13: The HCAL Barrel (HB), Endcap (HE) and Forward (HF) in the CMS Detector.

Barrel and Endcap

The Barrel (HB) of CMS HCAL is constructed of two half-barrels each of 4.3 m in length. The Endcap (HE) consists of two large structures, located at each end of the barrel detector and within the region of high magnetic field. Because the barrel HCAL inside the coil is not sufficiently thick to contain all the energy of high energy showers, additional scintillation layers (HOB) are placed just outside the magnet coil. The full depth of the combined HB and HOB detectors is approximately 11 absorption lengths.

The Central Hadron calorimeter is a sampling calorimeter, i.e. the shower develops in one of its medium while another medium is used to produce a signal proportional to the incident particle energy. The sampling calorimeter of HCAL consists of active material inserted between copper absorber plates. The absorber plates are 5 cm thick in the barrel and 8 cm thick in the endcap. The active elements of the entire central hadron calorimeter are 4 mm thick plastic scintillator tiles using wavelength-shifting (WLS) plastic fibers for read out operation.

The barrel hadron calorimeter is about 79 cm in depth. To ensure adequate sampling depth for the entire $\mid \eta \mid < 3.0$ region, the first muon absorber layer is instrumented with scintillator tiles to form an Outer Hadronic Calorimeter (HO).

Forward Calorimeter

The forward calorimeter (HF) extends the hermeticity of the central hadron calorimeter system to pseudorapidity $\eta = 5$, so that it meets a requirement for a good missing transverse energy measurement. The HF calorimeter covers the region $3.0 < \eta < 5.0$ and is built of steel absorber plates. Hadronic showers are sampled at various depths by radiation-resistant quartz fibers, which are inserted into the absorber plates. Because of the quartz fiber active element, it is predominantly sensitive to Cerenkov light from neutral pions which leads to its having a very localized response to hadronic showers.

The energy of jets is measured in a form of Cerenkov light signals produced as charged particles pass through the quartz fibers. These signals result princi-

pally from the electromagnetic component of showers, which results in excellent directional information for jet reconstruction.

Cerenkov light is emitted whenever a charged particle goes through matter with a velocity v exceeding the velocity of light in the medium. Fiber optics convey the Cerenkov signals to photomultiplier tubes which are located in radiation shielded zones to the side and behind each calorimeter.

Light from waveshifting fibers is sent via clear optical waveguide fibers to readout boxes located at the ends of the barrel and endcap detectors. For HCAL detector components positioned beyond the magnet coil, the readout boxes are located on the iron flux return beyond the muon system. Inside the readout boxes, the optical signals from various layers are aggregated into "towers" corresponding to $\Delta\eta \times \Delta\phi$ interval. These tower signals are measured and converted into fast electronic signals by photosensors. In the case of the barrel and endcap detectors, the photosensors are hybrid photodiodes (HPDs); and in the case of the forward detectors, the photosenseors are conventional photomultiplier.

3.2.5 The Muon Chamber

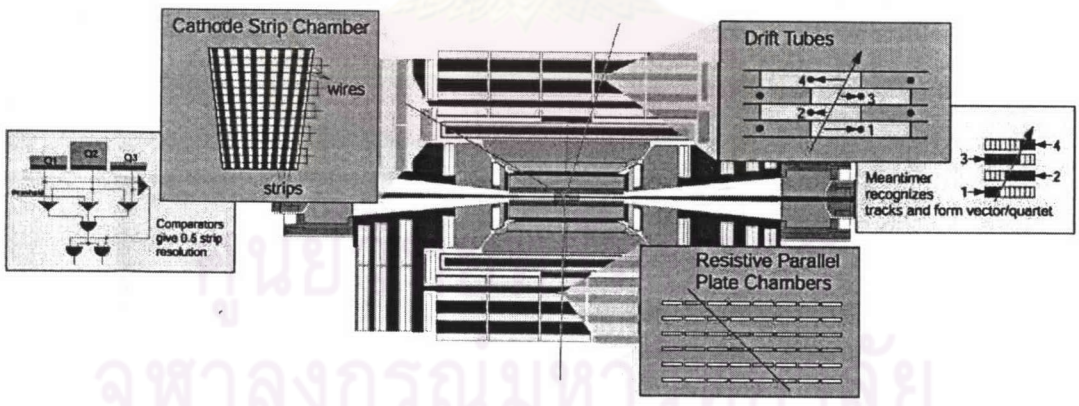

Figure 3.14: The CMS's Muon Chamber.

Muons are particles the CMS experiment is primarily dedicated to explore because their detection could provide clear distinction of signal over background which help determine a clear-cut signature for most of physics study. For example, the CMS program's "gold plated" signal is the Higgs bosons decay into $Z - Z$ or

$Z - Z^*$ and later decays into four charged leptons. For the case that the leptons are muons, the resolution of the mass of four particles cannot be too difficult to achieve since muons are less affected than electrons which suffer radiative losses in the tracker material. In a 150 GeV/c^2 Higgs event shown in Fig. 3.15, the muons are distinctly observed after the high magnetic field and absorbers filter out the large background of hadrons or non-isolated muons.

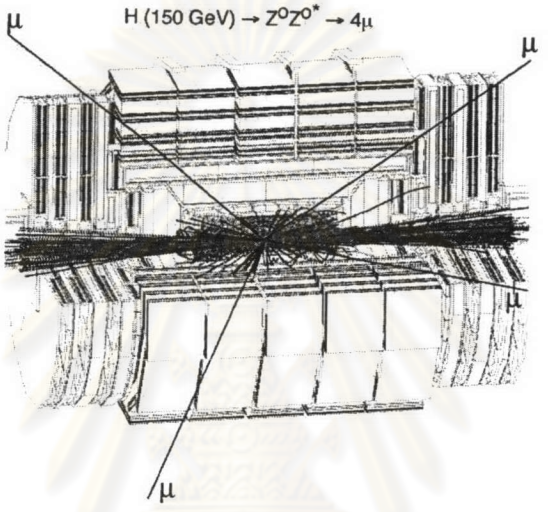

Figure 3.15: A 150 GeV Higgs event decaying into four muons in the CMS detector.

The muon system of the CMS detector, as shown in Fig. 3.14 incorporates three main functions: muon identification, muon trigger and muon momentum measurement.

Muons are identified by the large thickness of the absorber material (iron) of the Muon Chamber which allows the traverse of particles no other than neutrinos and muons. Before the first station of the calorimeters, there are at least 10 interaction lengths (λ); and before the last station, there are an additional 10λ of iron yoke. By lining up the hits in at least two out of the four muon stations, the identification of the muons can be achieved. The installation of multiple stations also enables the control of hadronic shower punch-through and hard muon bremsstrahlung.

With multiple chamber layers in each station, many distributed measurement points for building up a muon track pattern, as show in Fig. 3.16, can be

made without much difficulty.

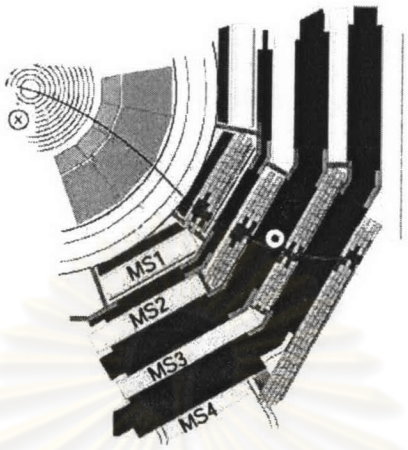

Figure 3.16: An example of muon tracks through the muon stations.

The muons' track is also not much disturbed by noise or background such as electrons from neutrons and photons. The thickness of the absorber between the stations also prevents station-to-station correlations due to high energy muon radiation.

For measuring the momentum of the muon, the magnetic field generated by the coil and conducted by the return yoke caused the track of charged particles to bend; and the momentum can be measured in similar way as explained in the Tracker section.

The muon trigger system helps identify muons and estimates their transverse momentum online. With high efficiency and precision, the system reduces the proton-proton interaction rate of $\sim$ 1 GHz to a few kHz by requiring that the transverse momentum of the muons must exceed a certain threshold.

In muon triggering operation, the electronics of the trigger rejects different types of background hits that can be mistaken as genuine, $high - P_T$ prompt muons. These backgrounds are generated from hadronic punch-throughs, debris from muon interactions with matter, thermal neutrons, beam halo in the forward direction and could also be noise in the electronics.

The CMS's muon system consists of three sub-detectors: Drift Tubes (DT) in the central barrel region, Resistive Parallel Plate Chambers (RPC) in both

the barrel and endcaps region and Cathode Strip Chamber (CSC) in the endcaps region. Below, we give brief explanation for each of the muon chamber's sub-detector.

Drift Tubes

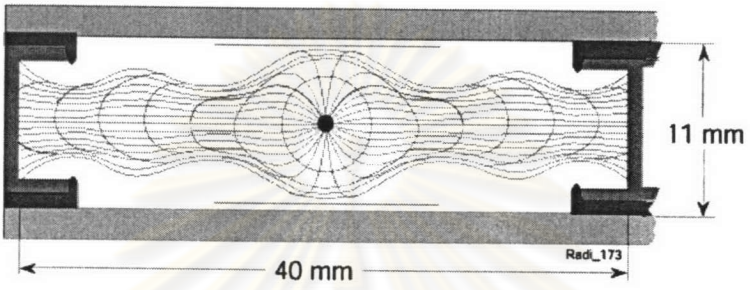

Figure 3.17: The Drift Tube of the Muon Chamber.

Drift Tubes (DT) contain a wire with large pitch (4 cm), and are assembled in layers. Some moderate numbers of electronic channels are in the DT for the read out electronics to record the signals that only be collected from the wires. Once a particle goes through the tube, it ionizes the gas in the tube and develops showers of electrons that will move toward the wire of positive potential. The positioning coordinate on the cross-sectional plane perpendicular to the wire is calculated from the time taken by the ionization electrons to drift toward the wire. Multiplying drift velocity of electrons in the gas with the amount of time taken by the drifted electrons, we can obtain the distance of particle from the wire. In an electric field, the drift velocity v_D is given by

$$v_D = \frac{e\tau E}{2m} \tag{3.3}$$

where e is charge, E is electric field, m is mass of electron and τ is a mean time between collisions. In the presence of a magnetic field B, the drift velocity is reduced, and the drift direction is no longer along the electric field; it is altered to

$$v'_D = v_D \cos \alpha_B, \tag{3.4}$$

where α_B is the drift angle given by,

$$\tan \alpha_B = 2Bv_D/E. \tag{3.5}$$

Here, we assume that B and E are orthogonal,

A DT layer is assembled by gluing layers of aluminium plate. To the aluminum plates, copper strips are glued in front of the wire to provide the electrostatic field of good shape. Most of the DT chamber is 2 m $\times$2.5 m in size, as shown in Fig. 3.17. The largest DT chamber in the CMS is 4 m $\times$2.5 m.

Cathode Strip Chambers

Cathode Strip Chambers (CSC) are multiwire proportional chambers composing of strips of segmented cathode plane running across wires. Once there are showers of particles developed on a wire, they will induce a charge on strips of the cathode plane. The two coordinates on a CSC plane is obtained from the independent detection of the signal induced by the same track on the strips and the wires at the same time. While the strips provide information on the ϕ angle (azimuthal angle), the wires provides information on the radial coordinate. Besides giving spatial and spacial measurement, the densely assembled wires of the CSC also make it a fast detector appropriate for triggering. The six layers inside the CSC modules provide rejection of non-muon background and a pattern recognition They also provide matching of internal track segments to external muon tracks.

In Fig. 3.18, the process of detecting the signal is displayed. Here, the electrons are first captured by the wire and positive ions are attracted toward the cathode. The process induces a current on the cathode strips perpendicular to the passage of particles.

In architectural consideration, the CSC is composed of six layers which are assembled in 7 Honeycomb panels; where one set of three plates provide support of two wire planes and the other sets of four plates give the etched strip. The two inner plates have strips on both faces, while the two outer plates have strips on only one face.

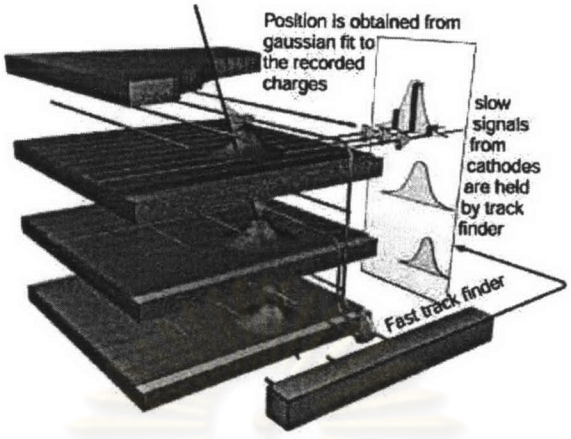

Figure 3.18: A sketch of the mechanism of signal detection in the CSCs.

Resistive Parallel plate Chambers

Resistive Parallel plate Chambers (RPC) are fast gaseous detectors. Besides giving a good spatial resolution, RPC gives an excellent time resolution of 1 ns. The RPC characteristics can be described as a parallel plate counter composed of two electrodes that is made from plastic material of very high resistivity. This design of RPC allows operation at a high rate which could achieve a high gas gain without causing catastrophic sparks or streamers. Thus, with this high gain, a very precise of little delay of passing time of an ionizing particle can be achieved. The RPC electrodes which have high resistivity are transparent to the electric signals originated from the current of the particle showers due to the shielding of external metallic strips. In the CMS Barrel, the strips are placed in parallel to the azimuthal angle and, in the Endcap CSCs, the strips are placed in parallel to the radial directions. This placement of the hit strips provides a measurement of the muon momentum that is used by Trigger.

From Fig. 3.19, inside the RPC, the electric field is uniform. Free electrons from ionizing particle close to the cathode gives a larger amount of secondary electrons in exponential multiplication. The cumulative effect of all the particle showers originates signals to be detected. By setting a proper threshold, the RPCs can detect signal which are dominantly electrons from the location close to the cathode. The time resolution, efficiency and time delay of the pulse are achieved by the threshold setting. Moreover, by choosing appropriate resistivity and plate

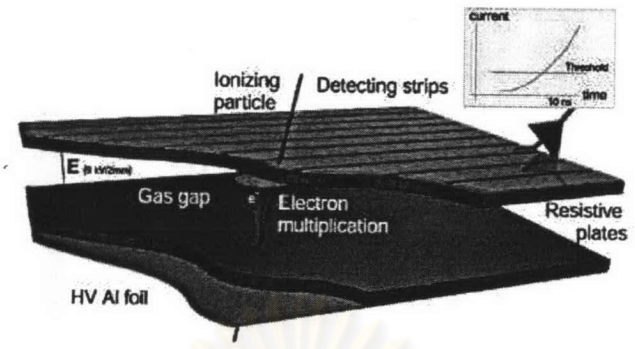

Figure 3.19: The sketch of detection process in the RPCs.

thickness, the RPC rate can achieve many thousand Hertz per cm^2.

3.2.6 Trigger and Data Acquisition

When the LHC starts operating, the two bunches of protons will cross each other at rate 40,000,000 times per second. At the highest luminosity of the particle beam, approximately 25 proton-proton collisions will be in each crossing. The Trigger and Data Acquisition System (TriDAS) of the CMS select, among those millions of events, about a hundred of the most interesting events per second, and then record them for the analysis study. Before going to TriDAS examination, the event has to be processed by two independent sets of Trigger Levels. The first level of the tests (Level-1 Trigger) is a simple test which requires short duration; but at the higher level (High Level Trigger 2, 3, ...), the operations are complicated algorithm and require significantly more time to run.

At Level-1 (LV1), special hardware processors is implemented to select signs of an interesting event, such as hits in muon chamber or some of calorimeter cells whose large amount of energy is deposited in them. The LV1 Trigger runs for less than one millionth of a second and selects the most interesting 100,000 events each second. After Level-1 accepts an event, the data for that event will be stored in 500 independent memories (RDPMs), of each connected to a different part of the CMS detector. A picture illustrated the Level-1 trigger system of the CMS is shown in Fig. 3.20

At Level-2, the TriDAS connects to more than one part of the detector. The

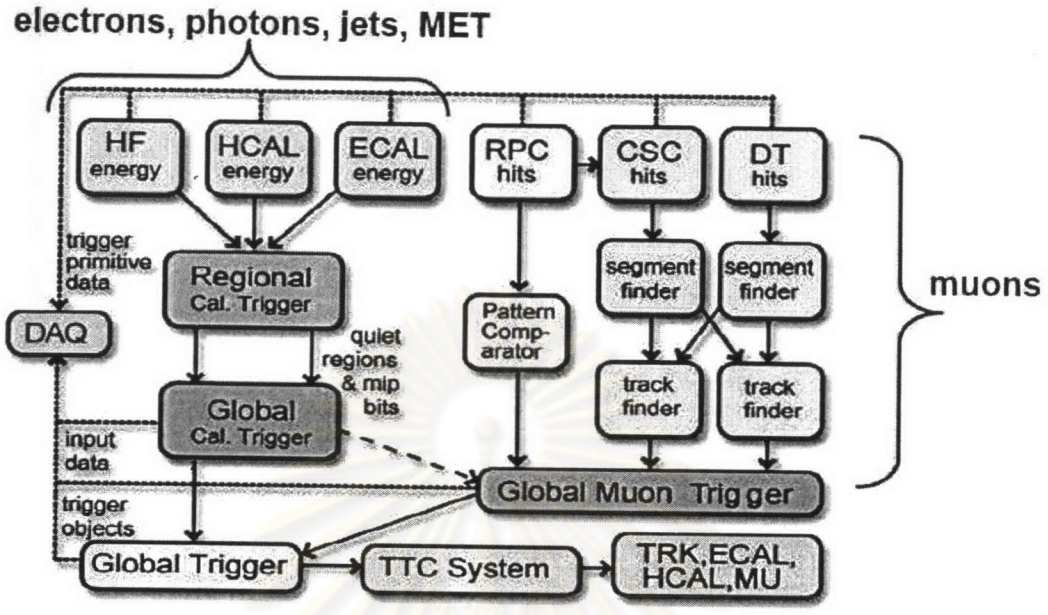

Figure 3.20: The CMS Level-1 trigger scheme. (picture from the CMS Collaboration, *The Trigger and Data Acquisition Project*, CERN/LHCC 2000-038.)

task of this level is to collect the data corresponding to the various pieces of the CMS detector and put them in a single location; the job is called event building. In CMS, there will be a large switch that will connect all 500 RDPMs to a farm of computers. This Trigger Level-2 will be run on processors commonly available for commercial.

Finally, at Level-3, the full event is put together, and an advanced level of physics algorithms can be applied to select for rare and complex signatures. This level of trigger is where the hits in the muon chambers are matched to particle tracks, and where a photon is identified as a cell with high electromagnetic energy and no track pointing to it. Throughout this process, the TriDAS system also monitors the CMS detector and corrects for any malfunction. A picture illustrated the CMS High-Level trigger is shown in Fig. 3.21

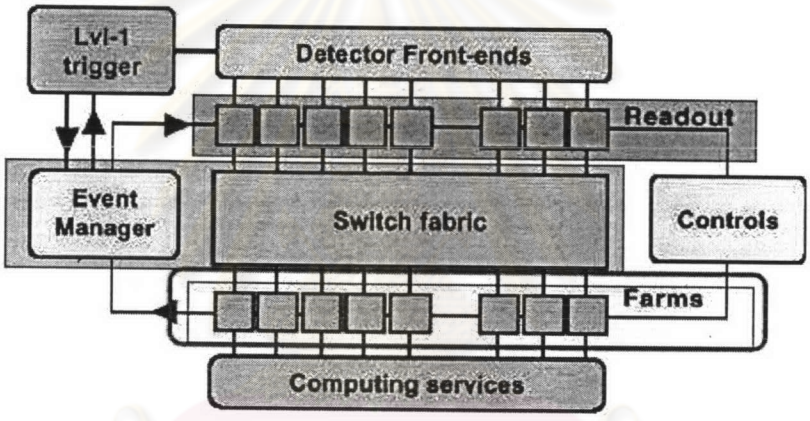

Figure 3.21: The CMS High-Level trigger scheme. (picture from the CMS Collaboration, *The Trigger and Data Acquisition Project*, CERN/LHCC 2000-038.)